Global aerosol optical properties and application to Moderate Resolution Imaging Spectroradiometer aerosol retrieval over land

Robert C. Levy,[1,2,3] Lorraine A. Remer,[2] and Oleg Dubovik[4]

Received 24 July 2006; revised 27 November 2006; accepted 6 April 2007; published 13 July 2007.

[1] As more information about global aerosol properties has become available from remotely sensed retrievals and in situ measurements, it is prudent to evaluate this new information, both on its own and in the context of satellite retrieval algorithms. Using the climatology of almucantur retrievals from global Aerosol Robotic Network (AERONET) Sun photometer sites, we perform cluster analysis to determine aerosol type as a function of location and season. We find that three spherical-derived types (describing fine-sized dominated aerosol) and one spheroid-derived types (describing coarse-sized dominated aerosol, presumably dust) generally describe the range of AERONET observed global aerosol properties. The fine-dominated types are separated mainly by their single scattering albedo (ω_0), ranging from nonabsorbing aerosol ($\omega_0 \sim 0.95$) in developed urban/industrial regions, to moderately absorbing aerosol ($\omega_0 \sim 0.90$) in forest fire burning and developing industrial regions, to absorbing aerosol ($\omega_0 \sim 0.85$) in regions of savanna/grassland burning. We identify the dominant aerosol type at each site, and extrapolate to create seasonal $1^\circ \times 1^\circ$ maps of expected aerosol types. Each aerosol type is bilognormal, with dynamic (function of optical depth) size parameters (radius, standard deviation, volume distribution) and complex refractive index. Not only are these parameters interesting in their own right, they can also be applied to aerosol retrieval algorithms, such as to aerosol retrieval over land from Moderate Resolution Imaging Spectroradiometer. Independent direct-Sun AERONET observations of spectral aerosol optical depth (τ) are consistent the spectral dependence of the models, indicating that our derived aerosol models are relevant.

Citation: Levy, R. C., L. A. Remer, and O. Dubovik (2007), Global aerosol optical properties and application to Moderate Resolution Imaging Spectroradiometer aerosol retrieval over land, *J. Geophys. Res.*, *112*, D13210, doi:10.1029/2006JD007815.

1. Introduction

[2] Tropospheric aerosols, also known as particulate matter, are produced by both natural and anthropogenic processes. Aerosols are major players within Earth's climate system [*Intergovernmental Panel on Climate Change* (*IPCC*), 2001], affecting the radiation budget, cloud processes, and surface air quality. As their lifetimes are on the order of days, aerosols are inhomogeneous in time and in space, with much higher concentrations near sources. Also, they vary in size by orders of magnitude and their properties change as they age and interact within the atmosphere. Thus it is extremely difficult to characterize aerosols on a global scale.

[3] This difficulty has not deterred attempts to quantify the nature of global aerosol properties and their effects. Physical, chemical, and optical properties of aerosols are routinely measured in the laboratory and in situ from all types of instruments, both from the ground and from aircraft. Unfortunately, these measurements perturb the aerosol field during collection and they are only measured at discrete points in space. Passive ground-based and airborne radiometers and Sun photometers provide measurements of the optical properties of ambient (nonperturbed) aerosol properties but also only at discrete locations. Few of these measurements offer insight into aerosol characteristics at remote locations. To link the discrete measurements to global processes (e.g., climate forcing), chemical transport models (CTM) and general circulation models (GCM) can be utilized [e.g., *IPCC*, 2001; *Kinne et al.*, 2006]. With the advent of calibrated, sophisticated satellite-borne radiometers, the aerosol community has been offered an observational dataset to bridge spatial gaps. These satellite radiometers (passive remote sensing) offer a much wider spatial view than traditional in situ or radiometric observations.

[4] While both observations and models can provide useful insight into the nature of aerosols and their effects,

[1]Science Systems and Applications Inc., Lanham, Maryland, USA.
[2]Laboratory for Atmospheres, NASA Goddard Space Flight Center, Greenbelt, Maryland, USA.
[3]Department of Atmospheric and Oceanic Science, University of Maryland, College Park, Maryland, USA.
[4]Laboratoire d'Optique Atmospherique, Université des Sciences et Technologies de Lille, Villeneuve d'Ascq, France.

Copyright 2007 by the American Geophysical Union.
0148-0227/07/2006JD007815

misunderstanding their information content can lead to incomplete or even erroneous conclusions. Ground-based and satellite-based measurements require different assumptions to infer aerosol properties, such that their results may seem contradictory yet both correct. For example, the correlation of satellite derived τ [no units] and PM2.5 surface concentration [μg/m^3] is being used for air quality forecast applications [e.g., *Chu et al.*, 2003; *Al-Saadi et al.*, 2005]. However, as these are very different physical parameters, it is imperative to evaluate surface/column apportionment and optics/mass relationships. Models require understanding of appropriate measurement assumptions/limitation, depending on which parameter is being evaluated. In other words, without properly documenting all assumptions, the collective worth of measurements and models will be compromised.

[5] In this paper, we derive characteristics of the global distribution of aerosols as observed by the ground-based radiometers (Sun photometers) of the Aerosol Robotic Network (AERONET) [*Holben et al.*, 1998]. We include all characteristics of the derived aerosol models, including lognormal modes, complex refractive index, resulting extinction/scattering coefficients and the like, such that they can be compared with observed characteristics from other datasets or implemented within models. Thus we leave a uniquely detailed "paper trail" of our efforts. We introduce the concept of passive remote sensing and Moderate Resolution Imaging Spectroradiometer (MODIS) aerosol retrieval in section 2. Section 3 describes the AERONET data used to develop the new models. Section 4 discusses cluster analysis of the AERONET data, fixing the aerosol type at given locations as a function of season, and the resulting optical extinction, scattering, and spectral τ dependence. In the conclusion (section 5) we describe how the aerosol models will be applied within the second generation MODIS aerosol retrieval algorithm.

2. Passive Remote Sensing From AERONET and MODIS

[6] Passive remote sensing of ambient tropospheric aerosol properties operates on the concept that solar radiation is modified as it interacts with the atmosphere (by gases and aerosols) and the surface [e.g., *Kaufman et al.*, 1997a]. The simplest conceptual measurement is retrieval of aerosol optical depth (AOD or τ) by observation of direct Sun extinction by a Sun photometer, such as done by AERONET. This measurement assumes that the radiation has had little or no interaction with the surface. When made at more than one wavelength (λ), observation of direct Sun extinction yield measurements of spectral (wavelength dependent) τ, which can yield estimates of the relative size of the ambient aerosol [e.g., *Eck et al.*, 1999; *O'Neill et al.*, 2003]. Requiring additional assumptions, properties of aerosol size distribution and scattering/extinction properties can be retrieved from measurements of spectral sky radiance [e.g., *Dubovik et al.*, 2000, 2002b]. Some of the assumptions relate to the shape of the aerosol (mixture of spherical and spheroids), surface properties, and parameterization of multiple scattering processes.

[7] Tropospheric aerosol properties may also be retrieved from satellite. Most satellite-derived aerosol datasets are created from measurements of backscattered radiation. Because the backscattered radiation includes multiple contributions from the atmosphere and surface, reasonable assumptions must be made to separate them. The upward spectral "reflectance" (normalized solar radiance) observed by a satellite at the top of the atmosphere (TOA) is a function of successive orders of radiation interactions within the coupled surface-atmosphere system. The observed spectral reflectance results in a combination of processes, including scattering of radiation within the atmosphere without interaction with the surface (known as the "atmospheric path reflectance"), the reflection of radiation off the surface that is directly transmitted to the TOA (the "surface function"), and the reflection of radiation from outside the sensor's field of view (the "environment function"). The environment function is neglected so that to a good approximation, the angular (function of solar zenith, sensor zenith, and Sun/sensor relative azimuth) TOA reflectance at a wavelength λ is described by

$$\rho^*_\lambda(\theta_0,\theta,\phi) = \rho^a_\lambda(\theta_0,\theta,\phi) + \frac{F_{d,\lambda}(\theta_0)T_\lambda(\theta)\rho^s_\lambda(\theta_0,\theta,\phi)}{1 - s_\lambda\rho^s_\lambda(\theta_0,\theta,\phi)}, \quad (1)$$

where ρ^a_λ represents the atmospheric path reflectance, including aerosol and molecular contributions, $F_{d\lambda}$ is the "normalized downward flux" for zero surface reflectance, T_λ represents "upward total transmission" into the satellite field of view, s_λ is the "atmospheric backscattering ratio" (reflectance of the atmosphere for istotropic light leaving the surface), and ρ^s_λ is the angular "surface reflectance" [*Kaufman et al.*, 1997b]. Except for the surface reflectance, each term on the right-hand side of equation (1) is a function of the aerosol type (chemical composition, size distribution) and its columnar loading (τ). Assuming well-defined spectral surface reflectance, accurate measurements of TOA spectral reflectance can lead to retrievals of spectral τ and reasonable estimates of one or more aerosol size parameters [e.g., *Tanré et al.*, 1996].

[8] In order to reduce the computational cost of difficult radiative transfer calculations at every satellite observed pixel, most, if not all, operational aerosol retrievals from satellite make use of a lookup table (LUT). The LUT is a simulation of the atmospheric contribution to the TOA reflectance, namely the nonsurface terms in equation (1). The LUT must be sufficiently representative of all reasonably likely atmospheric scenarios and satellite observations.

2.1. Ground-Based Measurements: AERONET

[9] The Sun photometers of AERONET provide a comprehensive data set of aerosol properties. Operating at more than hundreds of sites globally, AERONET has been reporting at some sites since 1993 (http://climate.gsfc.nasa.gov). "Sun" products are retrievals of spectral τ at several wavelengths (0.34, 0.38, 0.44, 0.67, 0.87, and 1.02 μm) resulting from observations of the spectral extinction of the direct sunbeam. They are provided at a minimum of every 15 min during the daytime. Angular distribution of sky radiances is measured at least at four wavelengths (0.44, 0.67, 0.87, and 1.02 μm) once every hour. (Some AERONET Sun photometers provide both sun sky measurements at more wavelengths). In addition, measurements of τ and sky radiances observed in the solar

almucantar are used for estimating detailed aerosol properties, such as aerosol size distribution, complex refractive index, phase function, absorption properties, etc. The retrieval algorithm approximates aerosol as an ensemble of polydisperse spheres [*Dubovik and King*, 2000] or randomly oriented spheroids [*Dubovik et al.*, 2002b] and provide the volume distribution ($dV/dlnR$) for 22 radius size bins and spectral complex refractive index (at wavelengths of sky radiances observations) that correspond to the best fit of both measured τ and sky radiances. The latest retrieval scheme [*Dubovik et al.*, 2006] assumes that aerosol is a mixture of spherical and nonspherical aerosol components and estimates the fraction that is nonspherical. The nonspherical fraction is modeled by ensemble of randomly oriented spheroids with distribution of aspect ratios retrieved [*Dubovik et al.*, 2006] by fitting scattering matrices of mineral dust measured in laboratory [*Volten et al.*, 2001]. (The same spheroid mixture is used in this study.) In either case, the modeling is performed using kernel lookup tables of quadrature coefficients employed in the numerical integration of spheroid optical properties over size and shape. These kernel lookup tables were generated using exact T-Matrix code [*Mishchenko and Travis*, 1994] and approximated geometric-optics-integral equation method of *Yang and Liou* [1996], that was used for size or shape parameters exceeded convergence limits of T-Matrix code. As a result the kernels cover wide range of sizes ($\sim 0.12 \leq 2\pi R/\lambda \leq \sim 625$) and axis ratios ε ($0.3 \leq \varepsilon \leq 3$). The usage of kernel lookup table allows quick and accurate simulations of optical properties of spheroids and therefore it allows using model of randomly oriented spheroids (introduced by *Mishchenko et al.* [1997] for desert dust) in AERONET operational retrievals.

[10] The retrieved size distribution and complex refractive index uniquely determine the aerosol radiative properties of phase function (P) and single scattering albedo (SSA or ω_0), also provided as retrieval products. In addition, AERONET derives optical properties (τ, P, and ω_0) and integral parameters of size distribution (volume concentration C_v, volume median radius r_v, and σ, standard deviation from r_v), separately for fine mode ($r \leq 0.6$ μm) and coarse mode ($r > 0.6$ μm) of the retrieved aerosol. Such representation of AERONET retrievals is based on the fact that majority of observed aerosol is bimodal and it is convenient for validation of satellite retrieval products, such as that of MODIS, whereas the parameters C_v, r_v, σ are simulated for each mode without assuming any particular shape of size distribution (see formulation in the work of *Dubovik et al.* [2002a]), they are analogous to corresponding parameters of log-normal size distributions. In fact, the assumption of log-normality allows accurate reproduction of aerosol optical properties in most cases, suggesting that these parameters represent log-normal properties of AERONET climatology [*Dubovik et al.*, 2002a].

[11] It should be noted that the retrievals from both Sun and Sky AERONET measurements are controlled by rigorous calibration and cloud screening processes. The results are also constrained by the criteria identified in sensitivity studies [*Dubovik et al.*, 2000]. As discussed by *Dubovik et al.* [2002a] these selections yield more accurate retrieval results, that can be used as ground-truth estimates (for certain aerosol properties). These products are known as Level 2 AERONET products, and within this paper we designate them as "L2A" products.

2.2. Satellite Measurements: MODIS

[12] The Moderate Resolution Imaging Spectroradiometer (MODIS) is one of the first passive satellite radiometers to be designed with aerosols in mind. Observing from approximately 700 km, it measures reflected solar radiance and terrestrial emission in 36 wavelength bands with resolutions between 250 m and 1 km. Nominally, it observes a swath ~2300 km, nearly covering the entire globe daily. Its measurements are organized into 5 min sections, known as "granules," each ~2300 km long. Since MODIS' launch aboard *Terra* (in late 1999) and aboard *Aqua* (in early 2002), MODIS spectral reflectance observations have led to retrievals of spectral τ and a measure of the aerosol size distribution, known as the nondust fraction or fine weighting (FW or η) in 10 km resolution (at nadir). Separate algorithms derive aerosol properties over ocean and land [e.g., *Remer et al.*, 2005], necessitated by different surface optical properties. MODIS data has been used in dozens of applications and publications since launch. Not only have MODIS aerosol products been used to answer scientific questions about radiation and climate [e.g., *IPCC*, 2001; *Yu et al.*, 2006], they are being used for applications such as monitoring surface air quality for health [e.g., *Chu et al.*, 2003; *Al-Saadi et al.*, 2005].

[13] The MODIS algorithm follows a lookup table (LUT) strategy, thereby assuming that a small set of aerosol types, loadings, and geometry can span the range of global aerosol conditions [e.g., *Kaufman et al.*, 1997b]. The algorithm then attempts to match the spectral reflectance observations with the LUT, theoretically retrieving the atmospheric scenario that produced the observed radiation field. The difficulty of course lies in making the most appropriate assumptions about both the surface and atmospheric contributions. The algorithms and products are continuously being evaluated, for self consistency and by comparison with other datasets, including AERONET [e.g., *Remer et al.*, 2005].

2.3. Aerosol Models and the MODIS LUT

[14] The MODIS aerosol algorithm over land chooses from a set of fine-dominated aerosol models and a single coarse-dominated aerosol model [e.g., *Kaufman et al.*, 1997b; *Remer et al.*, 2005]. The selection of which fine-dominated aerosol model is fixed based on season and location. The coarse-dominated model (dust) is considered fixed, globally. Early versions of the retrieval algorithm had a choice of two fine models [*Kaufman et al.*, 1997b], the "urban/industrial," and the "biomass burning/developing world," differing as to their refractive indices, single scattering albedos (SSA or ω_0), and phase functions. Each of these aerosol models is actually comprised of two or more lognormal modes [*Kaufman et al.*, 1997b], with their optical properties based on a combination of laboratory studies and Sun photometer data [e.g., *Remer and Kaufman*, 1998]. *Ichoku et al.* [2003] found that neither of the two fine models was sufficient to simulate the highly absorbing smoke seen over southern Africa. As a result, a third, empirically derived, "highly absorbing" fine model (with lower ω_0) was applied in Africa and other absorbing aerosol

regions [*Remer et al.*, 2005]. The addition of the "highly absorbing" model improved results in southern Africa.

[15] The optical parameters of the MODIS aerosol models were listed in multiple publications [e.g., *Kaufman et al.*, 1997b; *Remer and Kaufman*, 1998; *Remer et al.*, 2005], yet it has been over ten years since original algorithm development. We believe that MODIS should benefit from advances reported since then. We look to the AERONET climatology to help provide us with new models for MODIS.

2.4. Aerosol Models and AERONET

[16] As a test of the potential of updating the MODIS LUT, we began in the mid-Atlantic region of the U.S. East Coast. It was here that *Remer and Kaufman* [1998] used less than 150 AERONET retrievals, derived from earlier versions of almucantur retrieval [e.g., *Nakajima and King*, 1990; *Kaufman et al.*, 1994], to derive the urban/industrial aerosol model. Although this model was derived from data collected at only six sites in a concentrated area from Virginia to New Jersey, it was applied to the entire eastern half of North America and western Europe. Seven years later, *Levy et al.* [2005] demonstrated, empirically, that substituting AERONET climatology from the GSFC urban/industrial model [*Dubovik et al.*, 2002a] would help retrievals of high τ in the region.

[17] Although AERONET measures aerosol properties from the ground, we expect that its retrievals of aerosol optical properties can help to improve satellite retrievals in other regions, just like it helped for the U.S. East Coast. We look to the entire AERONET dataset to derive new global aerosol models and determine their geographical distribution.

[18] Coincident with our efforts, we learned that *Omar et al.* [2005] performed a cluster analysis of AERONET data and found that six aerosol models (listed as desert dust, biomass burning, background/rural polluted continental, marine, and dirty pollution) represent the global AERONET dataset. These models vary mainly by their ω_0 and size parameters. Two models are representative of very clean conditions (marine and background/rural). One of the models (dust) is coarse-dominated aerosol, and three are fine-dominated models having different ω_0 (biomass burning, polluted continental, and dirty pollution). While this study determines which models are represented at each AERONET site, it represents each site as a combination of multiple models and does not try to assign a type to each site, which is necessary for the global MODIS retrieval algorithm over land.

[19] Because the MODIS over-land retrieval employs only three channels, and suffers from surface and other contaminations, it is not sufficiently sensitive to aerosol ω_0 or details of the size distribution. However, these channels provide rough size information, which is used to estimate η (nondust fraction). For each retrieval, we give the algorithm the opportunity to mix one fine-dominated model with one coarse-dominated model for each retrieval, but the choice of models must be selected beforehand [e.g., *Kaufman et al.*, 1997b; *Remer et al.*, 2005]. This means that as a function of location (and time of year) the algorithm must designate unique fine- and coarse-dominated aerosol models. Unfortunately, the *Omar et al.* [2005] study leaves us one step short of this goal, since unique fine models were not found at every site. We must perform further analysis on the AERONET data to identify the appropriate model at each site. Since our goal is to apply AERONET data in the scope of global satellite aerosol retrieval, we perform a "subjective" cluster analysis to constrain the results to likely aerosol types.

3. Global Distribution of Aerosol Type

3.1. Subjective Cluster Analysis of AERONET Data

[20] For our subjective cluster analysis, we download about 136,000 L2A almucantur retrievals that were processed as of February 2005. At this time, the AERONET retrievals did not determine nonspherical fraction [e.g., *Dubovik et al.*, 2006], but instead assumed that either aerosol is 100% spherical or 100% spheroid mixture. We discriminate them by the minimum quality parameters suggested by the AERONET team, including τ at 0.44 μm greater than 0.4, solar zenith angle greater than 45°, 21 symmetric left/right azimuth angles, and radiance retrieval error less than 4%. The resulting data set is comprised of 13,496 spherical retrievals and 5128 spheroid retrievals (about 14% of the total). Keeping in mind our intended application to the MODIS aerosol algorithm, we perform quadratic fits to the spectral τ to estimate τ at 0.55 μm ($\tau_{0.55}$). In order to identify "dynamic" properties (function of τ [e.g., *Remer and Kaufman*, 1998]), we separate retrievals into ten equal bins of τ (having $\tau_{0.55}$ medians ranging between 0.28 and 1.33). Note that while we require $\tau_{0.44} > 0.40$, because of the strong spectral dependence in most cases, the minimum $\tau_{0.55}$ bin is 0.28. This is only slightly higher than the first aerosol entry of the MODIS LUT (0.25). For clustering, we employ the cluster analysis routines provided with the IDL (Interactive Display Language) software version 6.1. We cluster each τ bin separately to keep track of dynamic properties.

[21] In contrast to *Omar et al.* [2005], we desire to pursue not necessarily the most statistically significant clustering but rather to identify distinct models that could be useful for MODIS or other satellite algorithms. Knowing that MODIS is incapable of separating similar sized aerosol types over land, we chose to limit the number of possible aerosol types, to represent "low," "medium," and "high" in some parameter space. Thus we limit our cluster analysis to finding three clusters. We combine cluster results from separate τ bins, to collectively describe the dynamical properties of a particular aerosol type.

[22] From *Omar et al.* [2005] we learn that other than τ, unique aerosol types are identified by parameters that represent aerosol size and absorption. Since we are clustering within τ bins, we choose to cluster with respect to two optical parameters only SSA (ω_0) at 0.67 μm and the asymmetry parameter (ASYM or g) at 0.44 μm. In other words, one absorption parameter (ω_0) and one size parameter (g) is sufficient for representing the entire aerosol parameter space. We pick separate wavelengths because we do not want to accidentally create a dust cluster from near-ultraviolet 0.44 μm absorption (ω_0), while noting that larger-sized aerosols are be better separated by phase function asymmetry at the shortest wavelength (0.44 μm).

[23] Upon completion of our cluster analysis, we expect to find three aerosol types, each comprising about a third (plus or minus) of the entire AERONET population. However, we find two clusters with significant fraction and a third with only 11 points. This 11-point cluster includes points with unusually low $\omega_0 < 0.6$, and/or $g < 0.5$, indicating either retrieval errors or true outliers. We remove these points, recluster the rest, and now find three clusters, each having a similar number of points. We average the optical parameters within each cluster, to determine three distinct spherical fine-dominated aerosol optical models.

[24] As for the coarse aerosol model, we find that a single cluster describes the spheroid-based almucantur inversions [*Dubovik et al.*, 2006]. Since the sites contributing to spheroid data are primarily those known to be in dust regions, we presume that the spheroid model represents coarse-dominated (dust) aerosol.

3.2. Global Assignment of Aerosol Type

[25] Since the MODIS aerosol retrieval over land is not sufficiently sensitive to ω_0, the expected aerosol type must be assigned a priori to the retrieval. *Remer et al.* [2005] demonstrates how assumed aerosol type is assigned to region and season, even where little is known about the prevailing aerosol type. For example, MODIS assumes that smoke from tree forest fires (both tropical and high latitude forest) have similar optical properties as developing industrial regions in eastern Europe and most of Asia. We desire to use AERONET data to create similar maps that can be applied to satellite retrieval algorithms such as from MODIS.

[26] The first step is to determine the aerosol type that best represents each AERONET site. For each site, and for each season, we compute the percentage of the retrievals attributed to each cluster. Figures 1a–1d display pie plots at each site, as a function of season. To remove poor statistics, we show pie plots only at sites having at least 10 observations (per season) during the history of AERONET. Unfortunately, this excludes the many sites that have few retrievals of $\tau_{0.44} > 0.4$ ($\tau_{0.55} > \sim 0.28$). Green pie segments represent the nonabsorbing $\omega_0 \sim 0.95$ model (presumably urban/industrial aerosol), blue segments are the moderately absorbing $\omega_0 \sim 0.90$ model (presumably generic, forest smoke, and developing world aerosol), and red segments designate the highly absorbing $\omega_0 \sim 0.85$ model (presumably savanna/grassland smoke aerosol). At most sites and most seasons, the aerosol type is as expected. Nonabsorbing aerosol (green) dominates the U.S. East Coast and far western Europe, whereas highly absorbing aerosol (red) dominates the savannas of South America and Africa. Most other sites are either dominated by moderately absorbing aerosol (blue) or are a mix of all clusters.

[27] There are some surprises, however. Southeast Asia seems to be primarily nonabsorbing aerosols, as opposed to the absorbing aerosol assumed by *Remer et al.* [2005]. Recent studies [e.g., *Eck et al.*, 2005] confirm that aerosol in urban areas in far Southeast Asia are primarily nonabsorbing. A few sites in Western Europe have large fractions of absorbing aerosol, possibly a result of heavy diesel use.

[28] Keeping in mind our goal of dividing the world into plausible aerosol types, we require that each site should have an assumed aerosol type attached to it. The moderately absorbing aerosol type is set as the default, overwritten only if clear dominance of one of the other two aerosol types is observed. If either the nonabsorbing or the absorbing aerosol occupies more than 40% of the pie, while the other occupies less than 20%, we assign the site with the dominant aerosol type. For example, GSFC (39°N, 77°W) during the summer months (JJA), is 87% nonabsorbing and 13% moderately absorbing, meaning the nonabsorbing type is assigned.

[29] Figures 2a–2d display the aerosol types assigned at each site. As in Figure 1, green represents nonabsorbing, blue represents moderately absorbing, and red designates absorbing aerosol types. Most site designations seem reasonable and were expected from our experience. North America during the summer (JJA) is split between nonabsorbing and moderately absorbing aerosol types, much the same way (approximately −100° longitude) as was presented by *Remer et al.* [2005]. Southern Africa during the winter season (DJF) is solidly designated as absorbing aerosol [e.g., *Ichoku et al.*, 2003]. Western Europe is evenly split between nonabsorbing and moderately absorbing (except for two absorbing sites), meaning that a subjective decision was needed here. We chose to keep the region as "nonabsorbing" deferring to the assignment in the MODIS algorithm.

[30] Figure 3 plots the final assignment of aerosol types around the globe, as a function of season. Note that where possible the shapes correspond with the clustering of AERONET sites over land. At some regions, however, some subjectivity was needed to connect areas and draw lines. Over southeastern Asia, high mountains are boundaries between two aerosol regimes. Over Brazil, the boundary is near the border of Amazon forest and grasslands. Even though insufficient data exists for Africa north of the equator, the known surface types and seasonal cycles suggest that heavy absorbing aerosol would be produced during the biomass burning season. Red designates regions where the absorbing aerosol is chosen, whereas green represents nonabsorbing aerosol. The moderately absorbing ($\omega_0 \sim 0.90$) model is assumed everywhere else. These images were mapped onto a 1° longitude × 1° latitude grid, such that a fine aerosol type is assumed for each grid point, and each season. As new information becomes available, these maps can be easily updated.

4. Physical and Optical Properties of the Aerosol Models

4.1. Physical Properties

[31] The AERONET clustering produced three spherical, fine-dominated models (moderately absorbing, absorbing, and nonabsorbing), and one spheroid, coarse-dominated type (dust). We consider these to represent the range of expected global aerosol. By averaging the properties within each aerosol type cluster, we determine the physical properties of each aerosol "model." These models can be compared with the well-known "Continental" model [*Lenoble and Brogniez*, 1984] that is used in many satellite applications, including over-land applications of MODIS (e.g., ATBD-2006 for aerosol and the ATBD for MODIS land surface products).

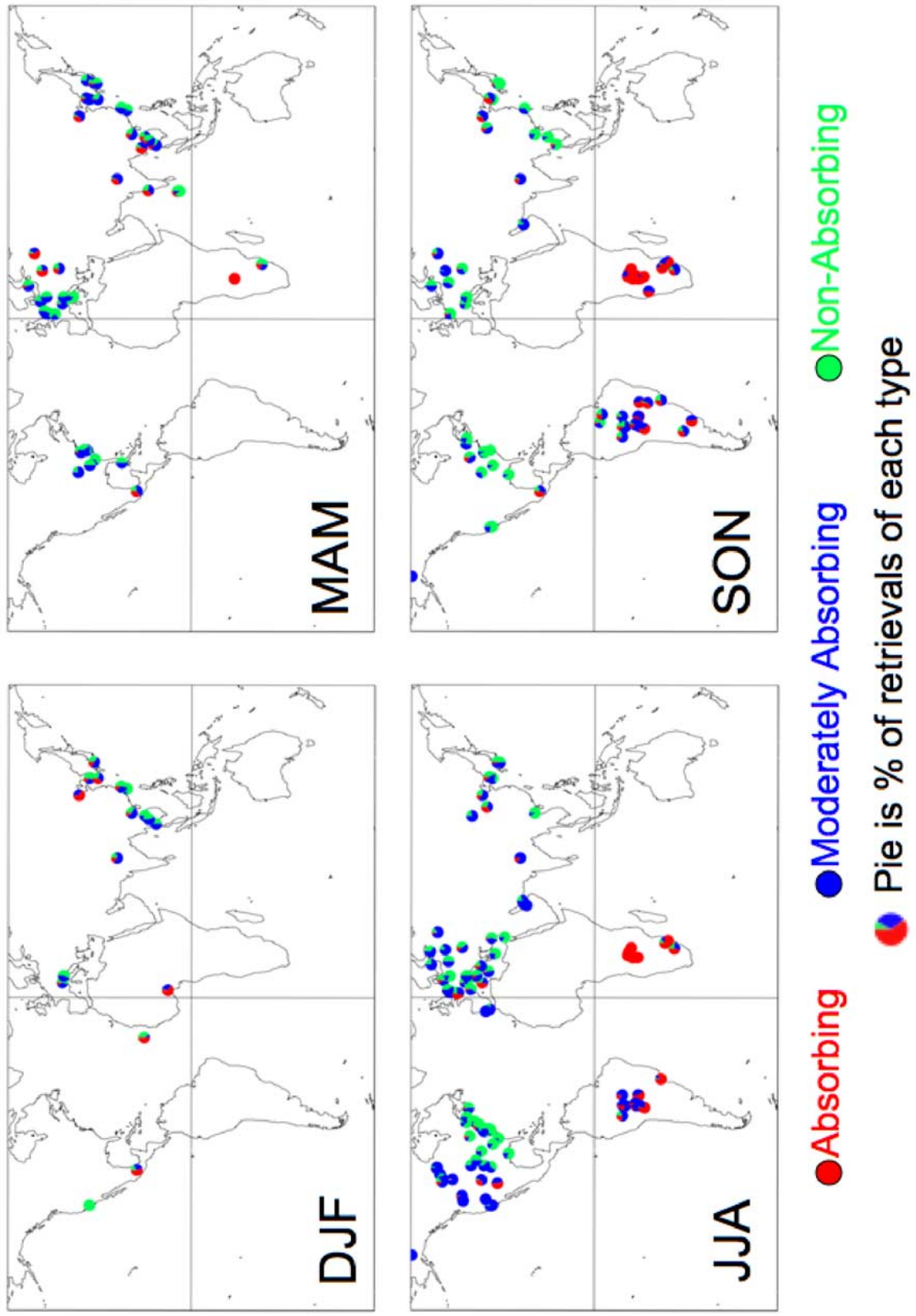

Figure 1. Percentage (pie charts) of spherical aerosol model type retrieved at each AERONET site per season. Colors represent absorbing ($\omega_0 \sim 0.85$), moderately absorbing ($\omega_0 \sim 0.90$), and nonabsorbing ($\omega_0 \sim 0.95$), respectively.

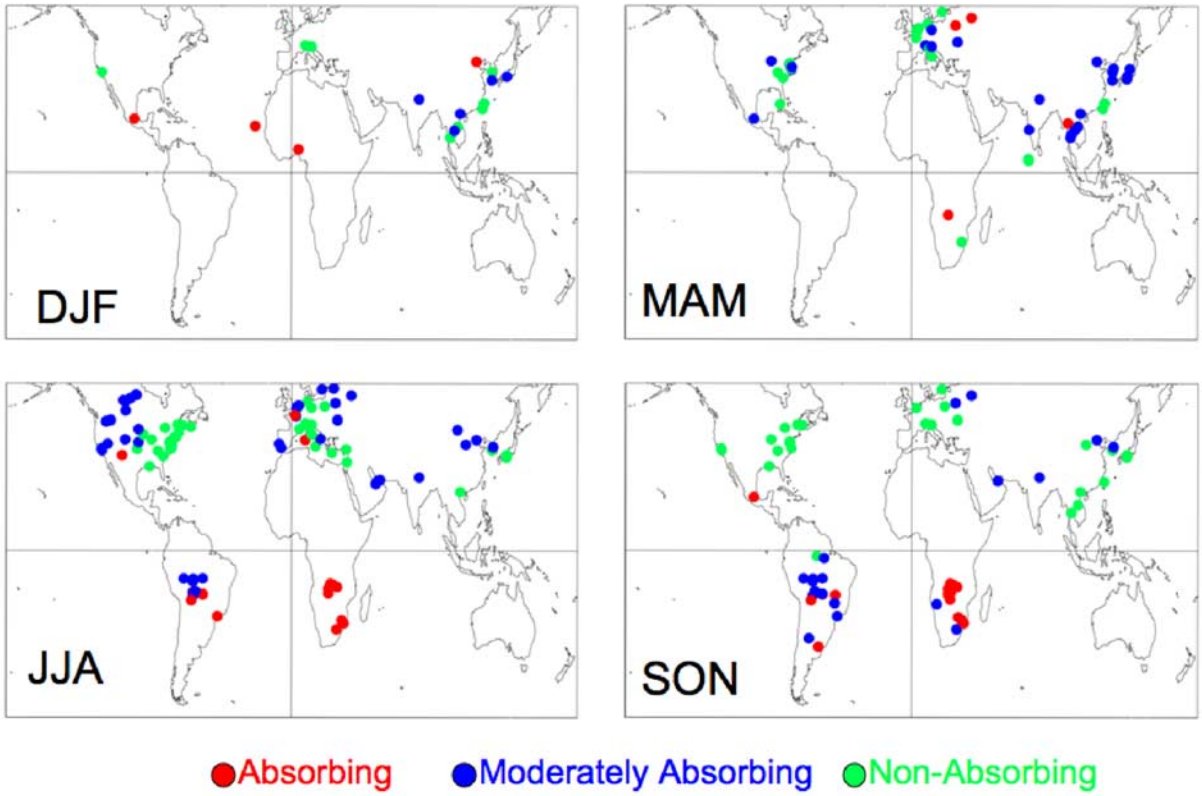

Figure 2. Final spherical aerosol model type designated at each AERONET site per season. Colors represent absorbing ($\omega_0 \sim 0.85$), moderately absorbing ($\omega_0 \sim 0.90$), and nonabsorbing ($\omega_0 \sim 0.95$), respectively.

[32] Figure 4 shows the size distributions for the four AERONET-derived models as a function of τ. Note the strong dynamic nature of the size properties of the nonabsorbing model, consistent with urban/industrial aerosol models [e.g., *Dubovik et al.*, 2002a; *Remer and Kaufman*, 1998]. While the primary product of the AERONET almucantur inversion is the complex refractive index and the volume size distribution $dV/dlnr$ in 22 bins of equal log size ($dlnr$), the AERONET retrieval reports the set of two lognormal modes that represent the size distribution. Table 1a displays the lognormal size parameters and refractive indices for the four AERONET-derived models, as well as the "Continental" model. For each lognormal mode, r_v is the median radius of the volume size distribution, σ is $\ln\sigma_v$ representing the standard deviation of the radius, and V_0 is the volume of particles per cross section of the atmospheric column (i.e., the amplitude of the lognormal size distribution).

4.2. Scattering and Extinction Properties

[33] For any size distribution of spherical particles, the number N is related to the volume V and area A distributions by:

$$\frac{dN}{d\ln r} = \frac{3}{4\pi r^3}\frac{dV}{d\ln r} = \frac{1}{\pi r^2}\frac{dA}{d\ln r}, \tag{2}$$

such that N_0, V_0, and A_0 are the amplitudes of the corresponding distributions, i.e.,

$$V_0 = \int_0^\infty \tfrac{dV}{d\ln r} d\ln r \quad N_0 = \int_0^\infty \tfrac{dN}{d\ln r} d\ln r \quad A_0 = \int_0^\infty \tfrac{dA}{d\ln r} d\ln r \tag{3}$$

and $dN/d\ln r$ is the number size distribution with r denoting radius (in μm). For a single lognormal mode, the median radius of the number distribution r_g is related to r_v by

$$r_g = r_v \exp\left(-3\sigma^2\right), \tag{4}$$

such that the number size distribution is

$$\frac{dN}{d\ln r} = \frac{N_0}{\sigma\sqrt{2\pi}} \exp\left(-\frac{\ln\left(r/r_g\right)^2}{2\sigma^2}\right) \quad \text{and} \quad N_0 = V_0 \frac{3}{4\pi r_g^3} \exp\left(-\frac{9}{2}\sigma^2\right). \tag{5}$$

The moments of order k, M^k are defined as

$$M^k = \int_0^\infty r^k \frac{dN}{d\ln r} d\ln r = \left(r_g\right)^k \exp\left(0.5\,k^2\sigma^2\right). \tag{6}$$

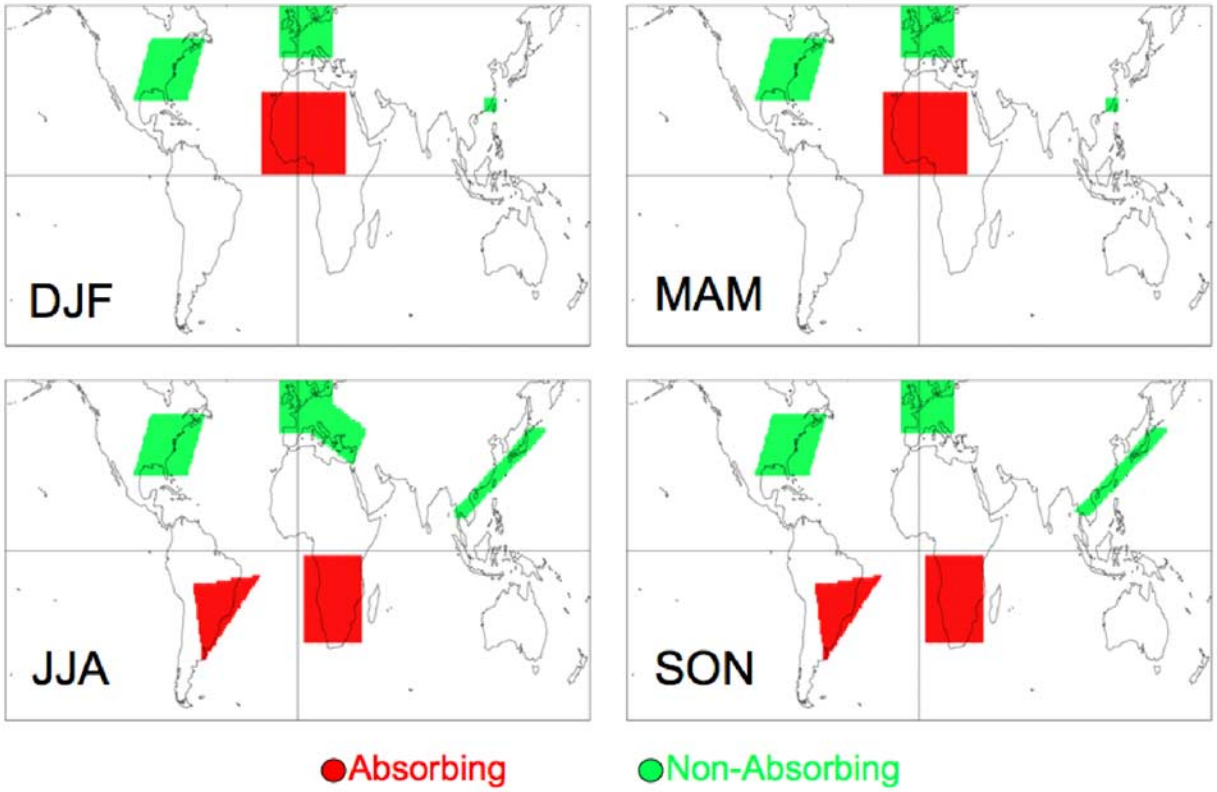

Figure 3. Final spherical aerosol model type designated at 1° × 1° gridbox per season. Red and green represent absorbing ($\omega_0 \sim 0.85$) or nonabsorbing ($\omega_0 \sim 0.95$) models, respectively. Moderately absorbing ($\omega_0 \sim 0.90$) is assumed everywhere else.

The effective radius r_{eff} in [μm] of a lognormal mode is

$$r_{eff} = \frac{M^3}{M^2} = \frac{\int_0^\infty r^3 \frac{dN}{d\ln r} d\ln r}{\int_0^\infty r^2 \frac{dN}{d\ln r} d\ln r} = \frac{3}{4}\frac{V_0}{A_0} = r_g \exp\left(\frac{5}{2}\sigma^2\right). \quad (7)$$

[34] For spherical particles, unitless extinction and scattering efficiencies, Q_{ext} and Q_{sca} of a single aerosol are defined by Mie theory to be related to the ratio of radius and wavelength and the complex refractive index of the particle. For our calculation we use the MIEV Mie code [*Wiscombe*, 1981], and assume that the distribution is normalized ($N_0 = 1$). The extinction/scattering efficiencies Q_{ext} and Q_{sca} for the particle population are defined by integrating the single particle efficiencies over the size distribution, specifically over approximately 350 bins of Mie size parameter (XX = $2\pi r/\lambda$) between 0.02 and 2000. The actual number of bins depends on how many are needed to represent 99.99% of the area distribution described by the lognormal mode.

[35] A Mie code is not appropriate for calculating the scattering and extinction properties of nonspherical particles [e.g., *Mishchenko*, 2002]. We use instead, the same kernel approach used for inverting AERONET almucanturs [*Dubovik et al.*, 2002b, 2006]. For spheroids, we assume a distribution of 11 spheroid aspect ratios between 0.4 and 2.48.

[36] Note, however, that since our aerosol models are composed of two or more lognormal modes, integration must be over both size bin and mode. For example, if there are two modes (i.e., modes 1 and 2), r_{eff} is

$$r_{eff} = \frac{\int_0^\infty r^3 \frac{(dN_1 + dN_2)}{d\ln r} d\ln r}{\int_0^\infty r^2 \frac{(dN_1 + dN_2)}{d\ln r} d\ln r}. \quad (8)$$

The extinction/scattering efficiencies for the aerosol model are calculated in similar fashion. The single scattering albedo for the model is the ratio of the scattering and extinction efficiencies (e.g., $\omega_0 = Q_{sca}/Q_{ext}$). The mass extinction coefficient B_{ext} is in units of (area per mass) and depends on Q_{ext} and the particle density ρ, i.e.,

$$B_{ext} = \frac{3Q_{ext}}{4\rho r_{eff}} \quad (9)$$

[*Chin et al.*, 2002]. This density should be appropriate for the aerosol type, but for model comparison, we assume 1 g/cm^3. We define the "mass concentration conversion factor" M_c, as the inverse of B, such that

$$M_c = \frac{1}{B_{ext}}. \quad (10)$$

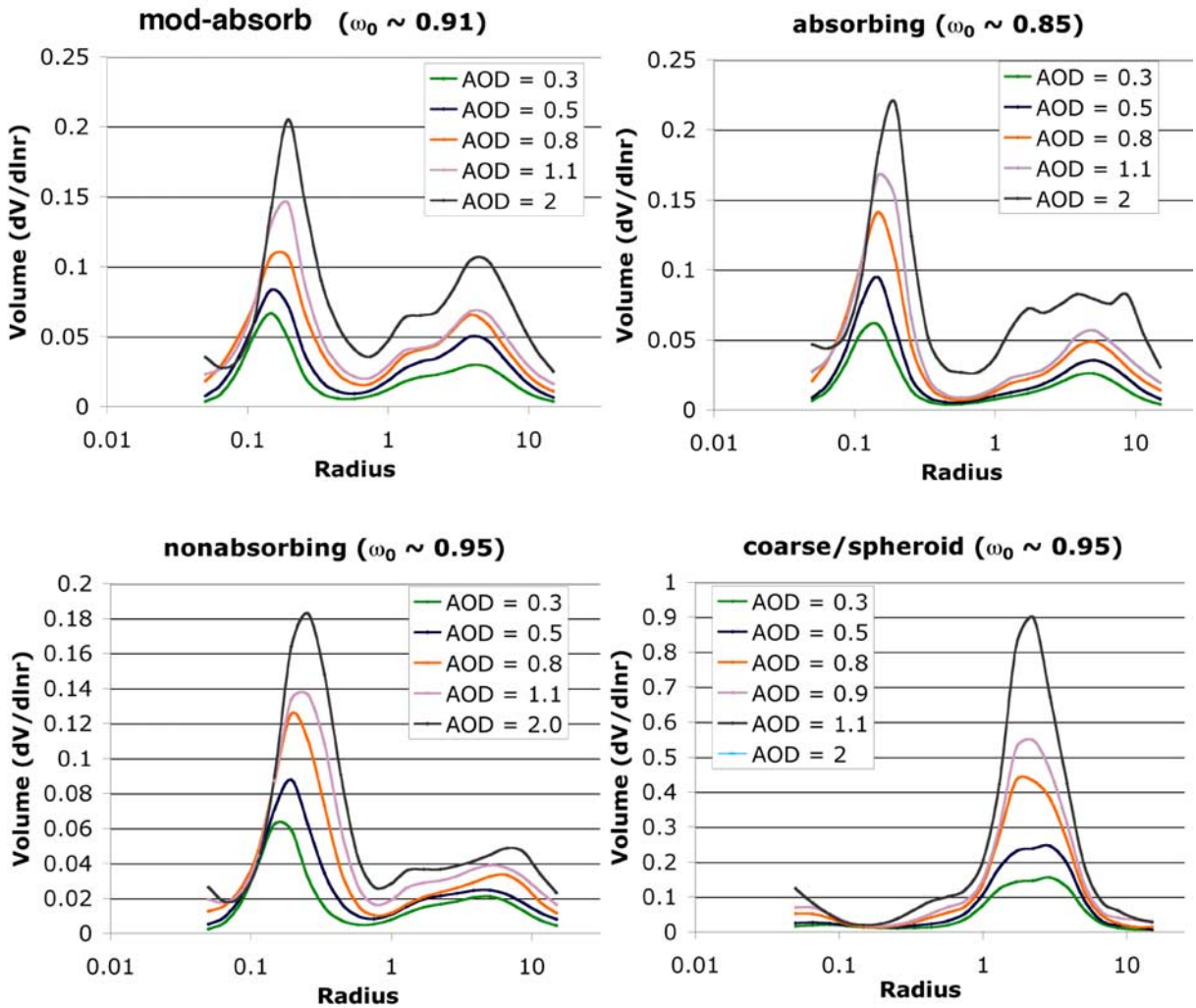

Figure 4. Aerosol size distribution as a function of τ (AOD) bin for the three spherical (moderately absorbing, absorbing, and nonabsorbing) and spheroid (dust) models identified by clustering of AERONET.

The columnar mass concentration, M (mass per area) is then

$$M = \tau M_c = \frac{\tau}{B_{ext}}. \tag{11}$$

[37] Since τ and B_{ext} are both defined as a function of wavelength, the columnar mass concentration is (as it should be) independent of wavelength. In reality, since the aerosol lognormal properties are dynamic (function of τ), that the extinction parameters and thus M_c is also a weak function of τ. Table 2 lists the extinction, scattering and mass conversion factors for the four AERONET-derived aerosol models, along with the Continental model for comparison. In each case, $\tau_{0.55}$ = 0.5.

[38] Figure 5 plots numerous properties of the four AERONET-derived aerosol models, along with the Continental model for comparison. Figures 5a–5d are plotted for $\tau_{0.55}$ = 0.5, where Figure 5a plots the spectral dependence of τ, Figure 5b plots phase function at 0.55 μm, Figure 5c plots the spectral dependence of ω_0., and Figure 5d plots the spectral dependence of g. Note that even though the three fine-dominated models have similar τ spectral dependence, they differ in other properties. The coarse model (spheroid-dust) has much smaller spectral dependence than any of the fine-dominated models, and nearly flat phase function in the 90°–180° scattering angle range observable by MODIS.

[39] Figure 6 compares the phase function of each of the models (also for $\tau_{0.55}$ = 0.5) as compared to the analogous models from the MODIS algorithm. Changes are minimal (especially for the 90°–180° scattering angle range) for the nonabsorbing (urban) and absorbing (heavy smoke) aerosol types. A possibly significant change is seen in the moderately absorbing (developing world/moderate smoke) phase function. The most significant change is for the "dust" model, due to assuming spheroids instead of spheres. The differences are primarily in the MODIS-observable scattering angle ranges, which could have a significant effect within the aerosol retrieval.

Table 1. Optical Properties of the Aerosol Models Used for the V5.2 Over-Land Lookup Table[a]

Model	Mode	r_v, μm	σ	V_0, $\mu m^3/\mu m^2$	Refractive Index: k
Continental					
	Water Solub	0.176	1.09	3.05	1.53 − 0.005i; 1
					1.53 − 0.006i; 2
					1.53 − 0.006i; 3
					1.42 − 0.01i; 4
	Dust	17.6	1.09	7.364	1.53 − 0.008i; 1
					1.53 − 0.008i; 2
					1.53 − 0.008i; 3
					1.22 − 0.009i; 4
	Soot	0.050	0.693	0.105	1.75 − 0.45i; 1
					1.75 − 0.44i; 2
					1.75 − 0.43i; 3
					1.81 − 0.50i; 4
Moderately Absorbing/Developing					
	Accum	$0.0203\tau + 0.145$	$0.1365\tau + 0.374$	$0.1642\ \tau^{0.775}$	$1.43 - (-0.002\tau + 0.008)i$
	Coarse	$0.3364\tau + 3.101$	$0.098\tau + 0.729$	$0.1482\ \tau^{0.684}$	$1.43 - (-0.002\tau + 0.008)i$
Absorbing/Smoke					
	Accum	$0.0096\tau + 0.134$	$0.0794\tau + 0.383$	$0.1748\ \tau^{0.891}$	1.51 − 0.02i
	Coarse	$0.9489\tau + 3.448$	$0.0409\tau + 0.743$	$0.1043\ \tau^{0.682}$	1.51 − 0.02i
Nonabsorb/Urban-Ind					
	Accum	$0.0434\tau + 0.160$	$0.1529\tau + 0.364$	$0.1718\ \tau^{0.821}$	$1.42 - (-0.0015\tau + 0.007)i$
	Coarse	$0.1411\tau + 3.325$	$0.1638\tau + 0.759$	$0.0934\ \tau^{0.639}$	$1.42 - (-0.0015\tau + 0.007)i$
Spheroid/Dust					
	Accum	$0.1416\ \tau^{-0.052}$	$0.7561\ \tau^{0.148}$	$0.0871\ \tau^{1.026}$	$1.48\tau^{-0.021} - (0.0025\tau^{0.132})i$; 1
					$1.48\tau^{-0.021} - 0.002i$; 2
					$1.48\tau^{-0.021} - (0.0018\tau^{-0.08})i$; 3
					$1.46\tau^{-0.040} - (0.0018\tau^{-0.30})i$; 4
	Coarse	2.2	$0.554\ \tau^{-0.052}$	$0.6786\ \tau^{1.057}$	$1.48\tau^{-0.021} - (0.0025\tau^{0.132})i$; 1
					$1.48\tau^{-0.021} - 0.002i$; 2
					$1.48\tau^{-0.021} - (0.0018\tau^{-0.08})i$; 3
					$1.46\tau^{-0.040} - (0.0018\tau^{-0.30})i$; 4

[a]Listed for each model are the individual lognormal modes, and the final SSA at different wavelengths. Listed for each mode are the volume modal radius r_v, standard deviation σ of the volume distribution, and total volume of the mode, V_0. The complex refractive index is assumed for all wavelengths (1, 2, 3, and 4 for 0.47, 0.55. 0.66, and 2.1 μm, respectively), unless otherwise noted. The absorbing and moderately absorbing model parameters (r_v, σ, and k) are defined for $\tau \leq 2.0$; for $\tau > 2.0$, we assume $\tau = 2.0$. Likewise, the nonabsorbing and spheroid model parameters are defined for $\tau \leq 1.0$. V_0 (for all models) is defined for all τ.

4.3. Spectral Dependence of τ Compared With AERONET "Sky" Retrievals

[40] How well do our derived models represent ambient aerosol at specific AERONET sites? For this purpose, we use the time series of Level 2 "Sun" retrieved products from AERONET, which are independent of the "sky" retrieved products. We cannot use the Sun measurements to evaluate the assumed absorption properties, but we can analyze the spectral dependence of the aerosol optical depth.

[41] Figure 5a showed the spectral τ dependence of each model for $\tau_{0.55} = 0.5$. Similar plots could be made from the spectral dependence indexed by other $\tau_{0.55}$ values. For each AERONET site, we separated retrievals into 3-month seasons (winter = DJF, spring = MAM, summer = JJA, fall = SON). Observations within each season were sorted according to $\tau_{0.55}$, where $\tau_{0.55}$ was calculated by fitting a quadratic to the observed spectral τ. For given indexed value of $\tau_{0.55}$ (τ = 0.25, 0.5, 1.0, 2.0), we determined which AERONET observation contained $\tau_{0.55}$ closest in magnitude to the indexed value. This we considered this location the "central" (C_i) index of the bin. The total number of observations "N_t" in each season, divided by 20, determined the number "N" of observations that should be considered close to the "central" index. Therefore the set of AERONET observations for the $\tau_{0.55}$ bin spanned between "C_i − N/2" and "C_i + N/2." If there were not enough observations near a certain $\tau_{0.55}$ value, we tried $N = N_t/40$. The spectral optical thickness for each bin was calculated by averaging the spectral optical thickness for the set of observations within the bin.

Table 2. Extinction/Mass Properties of the Aerosol Models[a]

Model	ω_0	Q_{ext}	r_{eff}, μm	B_{ext}, m^2/g	M_c, $\mu g/cm^2$
Continental	0.886	0.621	0.293	1.5910	62.8600
Moderately Absorbing/Developing World	0.920	1.018	0.261	2.9220	34.2230
Absorbing/Smoke	0.869	0.977	0.256	3.5330	28.3070
Nonabsorbing/Urban-Industrial	0.947	1.172	0.207	3.4310	29.1460
Spheroid/Dust	0.953	1.339	0.680	1.4770	67.6960

[a]Listed for each model are the single scattering albedo, extinction efficiency, effective radius, mass extinction coefficient, and mass concentration conversion factor. These parameters are calculated at 0.55 μm, for $\tau_{0.55} = 0.5$. The particle density is assumed to be 1 g/cm^3.

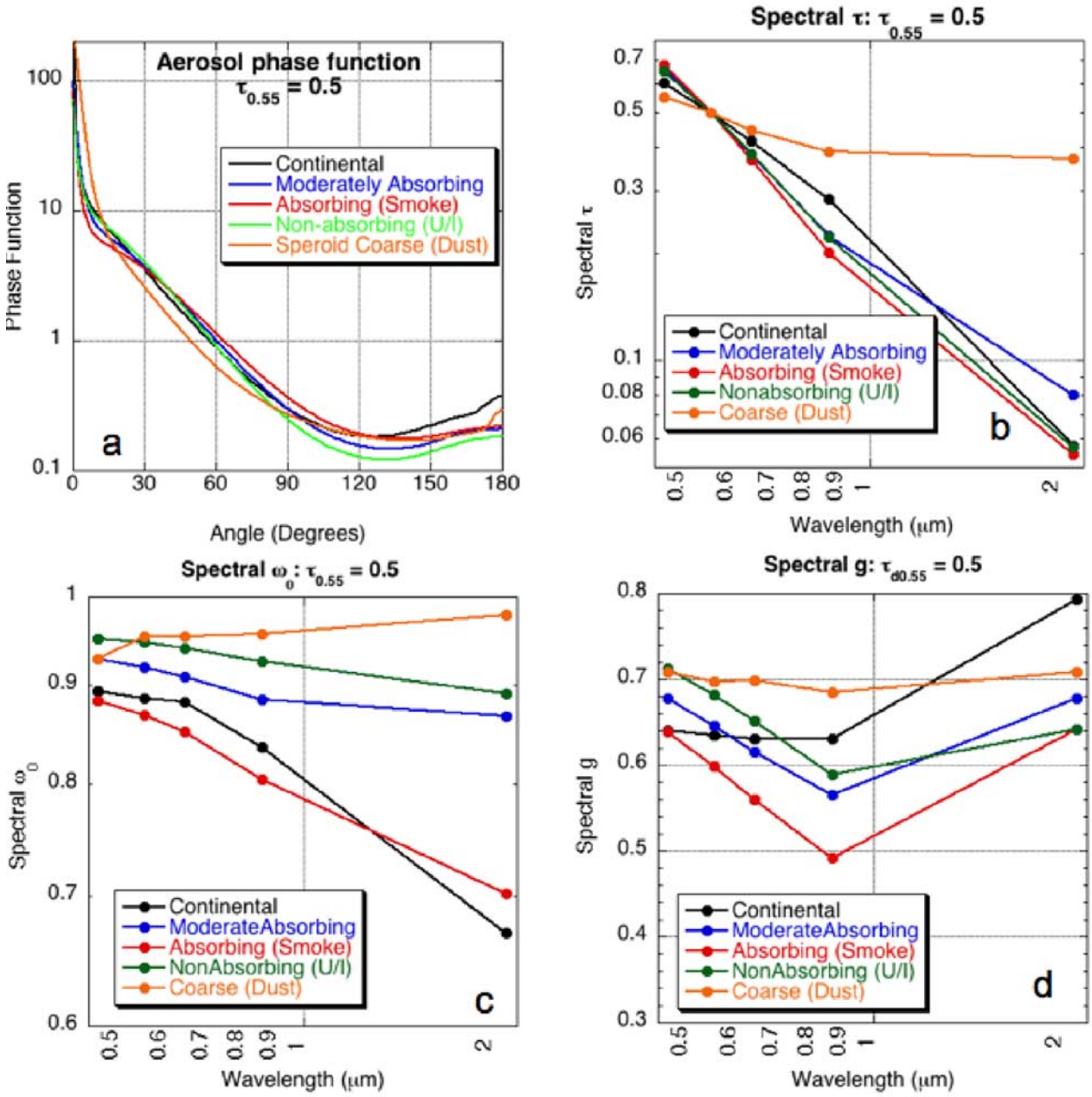

Figure 5. Optical properties of the AERONET-derived models, compared with the Continental model for $\tau_{0.55}$ = 0.5, showing (a) the phase function at 0.55 μm and the spectral dependence of (b) the optical depth, (c) single scattering albedo, and (d) asymmetry parameter.

[42] Figure 7 compares spectral dependence of the aerosol models with spectral dependence at selected AERONET sites, for indexed values of $\tau_{0.55}$ = 0.5. Since MODIS observes at many wavelengths (including 0.47, 0.55, 0.66, 0.86, and 2.12 μm bands), we interpolated AERONET (4 to 8 bands between 0.34 and 1.02 μm, depending on site) to the same wavelengths. Interpolation of AERONET to 2.12 μm was not performed because of the great distance from 1.02 μm. Different seasons (for AERONET) are represented by different line styles. At least one fine-dominated model, plus dust, is plotted for each site.

[43] At Alta Floresta (9°S, 56°W), the spectral dependence in the visible wavelengths agrees well with either the moderately absorbing or absorbing models. The AERONET spectral dependence varies with season, and we see this best at 0.86 μm. During the summer and fall, the AERONET dependence is slightly closer to the absorbing model than the moderately absorbing, and during the winter and spring, the moderately absorbing model provides a slightly better match to Sun-derived spectral τ. Our distribution of models includes this seasonal dependence at this location.

[44] At Cape Verde (16°N, 22°W), although the moderately absorbing fine-dominated model is assumed all year,

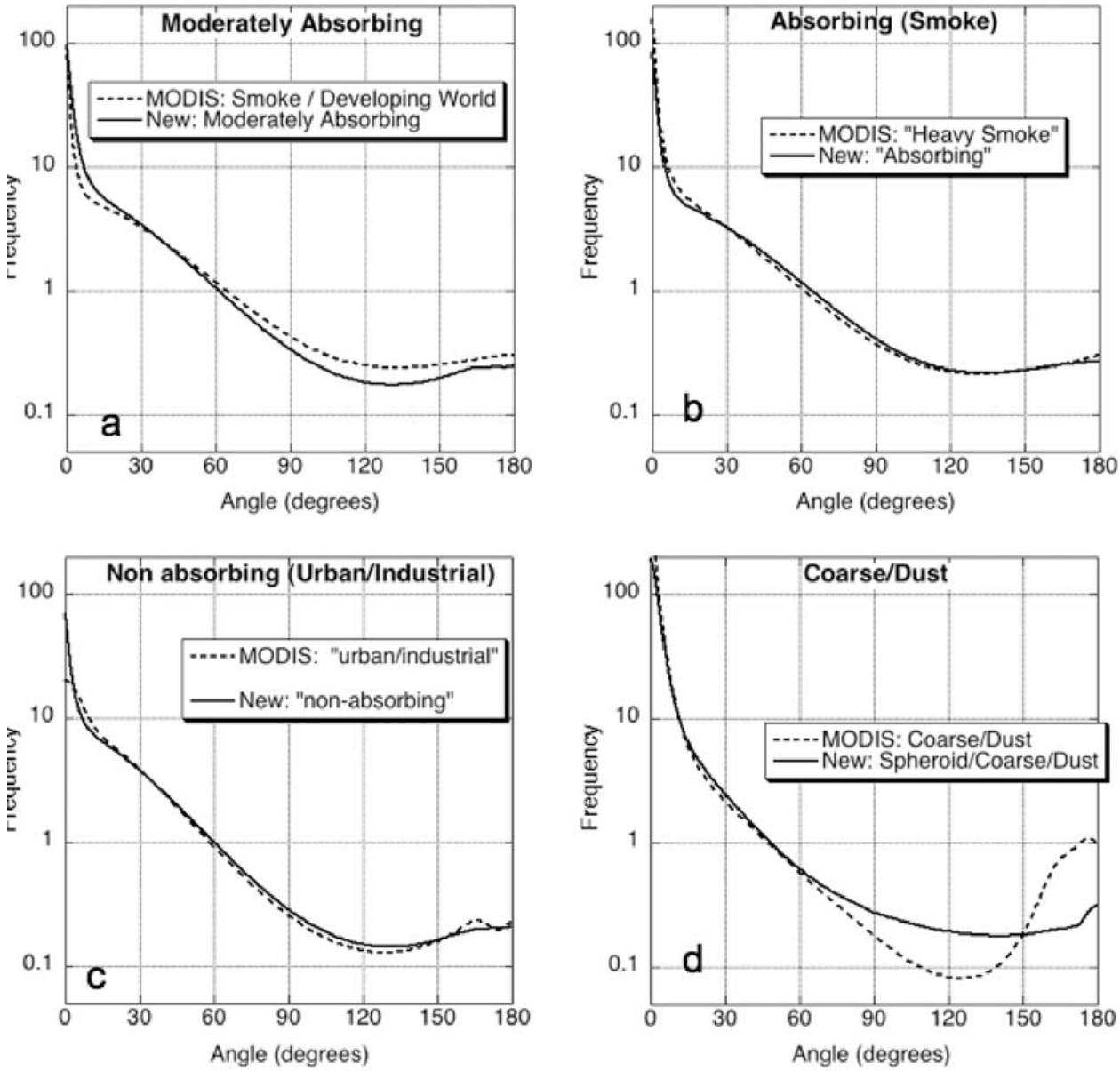

Figure 6. Comparison of phase function (at 0.55 μm) between new (solid curves) and analogous MODIS (dotted curves) aerosol models. Models are (a) moderately absorbing, (b) absorbing, (c) nonabsorbing, and (d) dust. For all plots, $\tau_{0.55} = 0.5$.

coarse (dust) is expected to dominate. Plotted for Cape Verde is the AERONET spectral τ compared with the modeled dust. Even though we believe that we have improved the dust model from that assumed by MODIS, the modeled spectral dependence is still too large to properly represent dust over Cape Verde.

[45] The nonabsorbing model ($\omega_0 \sim 0.95$) shows remarkable match to observations at GSFC (39°N, 77°W). The only difference is seen during the winter and spring for the lowest τ value (0.25), where the particles are known to be larger (have less spectral dependence) than the rest of the year. Mongu (15°S, 23°E) is another site that is well represented by its assumed aerosol type (absorbing).

[46] Beijing (39°N, 116°E) and Venice (45°N, 12°E) are interesting because dominant aerosol type is known to vary. Both sites are influenced by dust transport, so the averaged AERONET spectral dependence should lie somewhere between the fine-dominated and coarse-dominated (dust) models. It is clear that Beijing is mixed and is more coarse-dominated during the winter and spring. Venice is less often in the path of dust (from Africa) but its averaged spectral dependence shows the addition of coarse aerosol not represented by a fine-dominated model.

4.4. Relationship of Optical and Physical Properties: Application to PM2.5

[47] Satellite-derived τ (such as that of MODIS) is being used to retrieve surface $PM_{2.5}$ concentration, [$PM_{2.5}$], like that measured by the U.S. Environmental Protection Agency's AIRNow program [e.g., *Chu et al.*, 2003; *Al-Saadi*

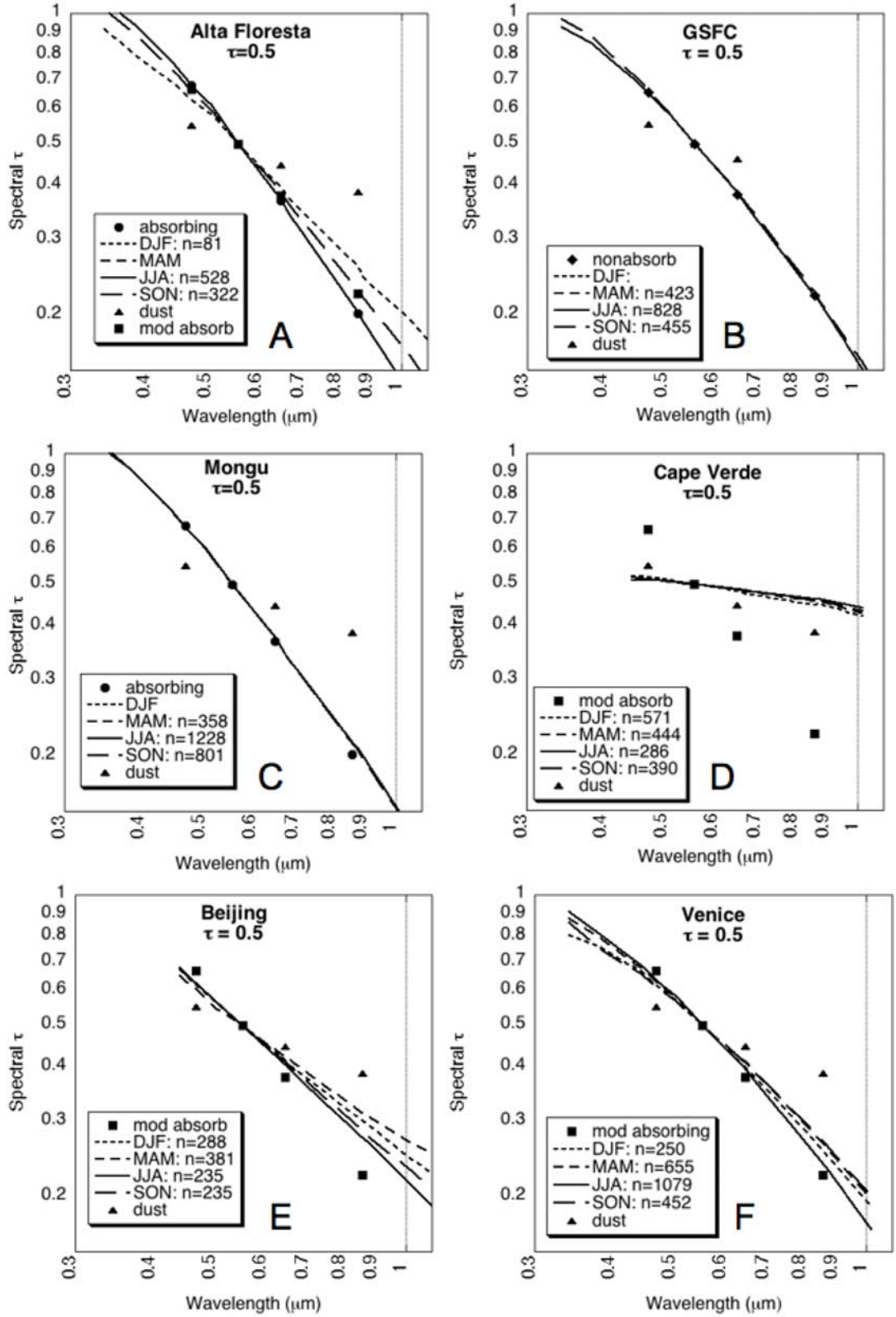

Figure 7. Comparison of spectral τ between new models (filled shapes) and averages of AERONET "Sun" measurements (dotted curves) at selected sites and seasons, for $\tau_{0.55}$ = 0.5. Different curves represent AERONET data during different seasons. The number of observations (n =) used to create each curve is displayed in the legend. Note that there are at least two aerosol types displayed (at least one fine-dominated type plus dust). Sites plotted are (a) Alta Floresta, (b) GSFC, (c) Mongu, (d) Cape Verde, (e) Beijing, and (f) Venice.

et al., 2005]. Of course, τ and $[PM_{2.5}]$ are very different physical quantities; τ being an optical property that represents the instantaneous integrated ambient vertical column, whereas $[PM_{2.5}]$ represents a time-averaged point near the surface and dried. These products will only be related if the bulk of the aerosol column is located near the surface. To relate the two quantities, one strategy is to estimate $[PM_{2.5}]$ based on empirical comparison with τ. Over the eastern U.S. during the summer, where and when most of the aerosol is near the surface, correlation between the two products is on the order of $R = 0.6$ [*Al-Saadi et al.*, 2005], suggesting that the satellite data contains information for air quality monitoring and forecasting. Estimates for the AOD-to-mass conversion factor over the eastern U.S. range between 25 and 60 [μg/m$^3/\tau$] depending on conditions (J. Engel-Cox, personal communication, 2007).

[48] Using some appropriate assumptions, however, one could derive a more physical link between the two quantities. To paraphrase *Koepke et al.* [1997], the aerosol models we have developed here must be consistent with the mass and optical properties of aerosol, measured in situ as well as remotely sensed. We use the case of aerosol over the eastern U.S. to understand the AOD-to-mass conversion factor.

[49] As shown in Table 2, $\tau_{0.55} = 0.5$ of the nonabsorbing aerosol model has $B_{ext} = 3.43$ m^2/g and $M_c = 29.14$ μg/cm$^2/\tau$. Owing to the dynamic function of τ, $\tau_{0.55} = 1.0$ of the same model results in $B_{ext} = 3.73$ m^2/g, and $M_c = 26.84$ μg/cm$^2/\tau$. Note that the particle density is assumed as $\rho = 1$ g/cm^3, and that our values are for a wavelength of 0.55 μm. These parameters were estimated by integrating Mie code results over ~350 bins of radius (~0.001–40 μm), which should be close to any "theoretical" integrated values.

[50] To convert M_c to surface $[PM_{2.5}]$, we require assumptions about boundary layer height, dry particle density, aerosol type hygroscopicity, and effect of measurement size cutoff compared to the theoretical size distribution. The equation looks something like:

$$[PM_{2.5}] = \frac{\rho'}{\Delta Z_{PBL} F} \tau M_c' \tag{12}$$

where ρ' is the magnitude of the density of dry particles (ratio to unity), F is a "hygroscopic factor" appropriate for the aerosol type and ambient relative humidity and ΔZ_{PBL} is the thickness of the boundary layer. M_c' is a mass conversion coefficient appropriate for the measured size distribution, which in case of $PM_{2.5}$ are aerosols less than 2.5 μm in diameter (radius < 1.25 μm). Note the necessity of performing correct unit conversion to get $[PM_{2.5}]$ in units of [μg/m^3].

[51] The density for sulfate-dominated aerosol is on the order of 1.7 g/cm^3 [e.g., *Koepke et al.*, 1997], and the height of the convective boundary layer is on the order of 3 km during haze events [e.g., *Taubman et al.*, 2006]. The hygroscopic factor, F, is related to absorption of water vapor by aerosol in high relative humidity (RH) conditions and represents the ratio of aerosol scattering in ambient relative humidity (RH ~ 80%) versus when dried (RH ~ 30%). For aerosol over the eastern U.S., F is on the order of 2 [e.g., *Gassó and Hegg*, 2003]. The last piece of the puzzle relates to the definition of $[PM_{2.5}]$, which is a measure of particles with diameters less than 2.5 μm, (r < 1.25 μm). There may be a significant difference between the measured and the actual (theoretical Mie) mass concentration [e.g., *Koepke et al.*, 1997]. Any addition of large particles will increase the theoretical total mass without affecting the aerosol optical properties in visible wavelengths. When we calculate Mie scattering/efficiency parameters only between 0.01 and 1.25 μm, instead of over the entire Mie size range, M_c' is about 25% less than M_c. The combination of all terms in this equation leads to a theoretical AOD-to-mass conversion factor over the eastern U.S. range of about 56 [μg/m$^3/\tau$], well within the observed range of conversion factors.

5. Conclusion

[52] Since 2000, MODIS has been operationally retrieving aerosol properties over land. However, during the process of MODIS algorithm evaluation, we determined the need to update the set of assumed aerosol models. We used the entire time series of almucantur-derived aerosol properties from all AERONET sites to compose a set of three fine-dominated (spherical) and one coarse-dominated (spheroid) aerosol optical models that represent range of likely and observable global aerosol conditions. The fine-dominated aerosol types differ mainly by their values of ω_0, "moderately absorbing" ($\omega_0 \sim 0.90$), "absorbing" ($\omega_0 \sim 0.85$), and "nonabsorbing" ($\omega_0 \sim 0.95$). We then created seasonal 1° × 1° maps of assigning aerosol type to each grid.

[53] We used Mie code (for spherical aerosols) and T-matrix kernel code (for spheroids) to compute extinction and scattering properties of the aerosol models. Phase functions for the fine-dominated models were similar to those assumed within the operational MODIS algorithm. The coarse-dominated model had substantially different phase function from the MODIS-assumed dust, due to the assumption of spheroids instead of spheres. Spectral dependence of τ of the models was compared with "Sun" retrieved observations from selected AERONET sites. Sites dominated by fine aerosol (e.g., GSFC and Mongu) were well represented by their assumed aerosol type. At Alta Floresta, also dominated by fine aerosol, our seasonal choice of fine models (moderately absorbing versus absorbing) was correct. In a dust-dominated site such as Cape Verde, our dust model is an improvement to previous versions but still has too much spectral dependence. Sites that are influenced by occasional dust episodes (e.g., Venice or Beijing) show spectral dependence between that of the fine- and coarse-dominated models. Such mixtures are within the capacity of the MODIS algorithm to retrieve. Using appropriate assumptions about size cutoffs, density, humidification, and boundary layer heights, we were able to relate the nonabsorbing aerosol optical model to surface $PM_{2.5}$ concentration over the eastern U.S.

[54] The derivation of the new set of aerosol models provides important information on characterizing the global aerosol system. Details about their derivation are important for comparison with measurements from other sensors and with models. These models will be implemented within the new aerosol algorithm [*Levy et al.*, 2007] and are expected to improve the accuracy of the aerosol retrieval over land.

[55] **Acknowledgments.** We would like to thank Tom Eck and the rest of the AERONET team for being available for questions, to Santiago Gassó for advice on humidification and other complications, and to Jennifer Hains for help with cluster analysis. We also are grateful for the efforts of our anonymous reviewers.

References

Al-Saadi, J., et al. (2005), Improving national air quality forecasts with satellite aerosol observations, *Bull. Am. Meteorol. Soc.*, *86*(9), 1249–1261.

Chin, M., et al. (2002), Tropospheric aerosol optical thickness from the GOCART model and comparisons with satellite and Sun photometer measurements, *J. Atmos. Sci.*, *59*(3), 461–483.

Chu, D. A., Y. J. Kaufman, G. Zibordi, J. D. Chern, J. Mao, C. Li, and B. N. Holben (2003), Global monitoring of air pollution over land from EOS-Terra MODIS, *J. Geophys. Res.*, *108*(D21), 4661, doi:10.1029/2002JD003179.

Dubovik, O., and M. D. King (2000), A flexible inversion algorithm for retrieval of aerosol optical properties from Sun and sky radiance measurements, *J. Geophys. Res.*, *105*, 20,673–20,696.

Dubovik, O., et al. (2000), Accuracy assessments of aerosol optical properties retrieved from AERONET Sun and sky radiance measurements, *J. Geophys. Res.*, *105*, 9791–9806.

Dubovik, O., et al. (2002a), Variability of absorption and optical properties of key aerosol types observed in worldwide locations, *J. Atmos. Sci.*, *59*(3), 590–608.

Dubovik, O., et al. (2002b), Non-spherical aerosol retrieval method employing light scattering by spheroids, *Geophys. Res. Lett.*, *29*(10), 1415, doi:10.1029/2001GL014506.

Dubovik, O., et al. (2006), Application of light scattering by spheroids for accounting for particle nonsphericity in remote sensing of desert dust, *J. Geophys. Res.*, *111*, D11208, doi:10.1029/2005JD006619.

Eck, T. F., et al. (1999), Wavelength dependence of the optical depth of biomass burning, urban, and desert dust aerosols, *J. Geophys. Res.*, *104*, 31,333–31,349.

Eck, T. F., et al. (2005), Columnar aerosol optical properties at AERONET sites in central eastern Asia and aerosol transport to the tropical mid-Pacific, *J. Geophys. Res.*, *110*, D06202, doi:10.1029/2004JD005274.

Gassó, S., and D. A. Hegg (2003), On the retrieval of columnar aerosol mass and CCN concentration by MODIS, *J. Geophys. Res.*, *108*(D1), 4010, doi:10.1029/2002JD002382.

Holben, B. N., et al. (1998), AERONET - A federated instrument network and data archive for aerosol characterization, *Remote. Sens. Environ.*, *66*(1), 1–16.

Ichoku, C., et al. (2003), MODIS observation of aerosols and estimation of aerosol radiative forcing over southern Africa during SAFARI 2000, *J. Geophys. Res.*, *108*(D13), 8499, doi:10.1029/2002JD002366.

Intergovernmental Panel on Climate Change (IPCC) (2001), *Climate Change 2001: The Scientific Basis*, edited by J. T. Houghton et al., 944 pp., Cambridge Univ. Press, New York.

Kaufman, Y. J., A. Gitelson, A. Karnieli, E. Ganor, R. S. Fraser, T. Nakajima, S. Mattoo, and B. N. Holben (1994), Size distribution and scattering phase function of aerosol particles retrieved from sky brightness measurements, *J. Geophys. Res.*, *99*, 10,341–10,356.

Kaufman, Y. J., D. Tanre, H. R. Gordon, T. Nakajima, J. Lenoble, R. Frouin, H. Grassl, B. M. Herman, M. D. King, and P. M. Teillet (1997a), Passive remote sensing of tropospheric aerosol and atmospheric correction for the aerosol effect, *J. Geophys. Res.*, *102*, 16,815–16,830.

Kaufman, Y. J., et al. (1997b), Operational remote sensing of tropospheric aerosol over land from EOS moderate resolution imaging spectroradiometer, *J. Geophys. Res.*, *102*, 17,051–17,067.

Kinne, S., et al. (2006), An AeroCom initial assessment—Optical properties in aerosol component modules of global models, *Atmos. Chem. Phys.*, *6*, 1–20.

Koepke, P., M. Hess, I. Schult, and E. P. Shettle (1997), Global aerosol data set, *Rep. 243*, Max-Planck-Inst. für Meteorol., Hamburg, Germany.

Lenoble, J., and C. Brogniez (1984), A comparative review of radiation aerosol models, *Beitr. Phys. Atmos.*, *57*(l), 1–20.

Levy, R. C., et al. (2005), Evaluation of the MODIS aerosol retrievals over ocean and land during CLAMS, *J. Atmos. Sci.*, *62*(4), 974–992.

Levy, R. C., L. A. Remer, S. Mattoo, E. Vermote, and Y. J. Kaufman (2007), The second generation operational algorithm for retrieving aerosol properties over land from MODIS spectral reflectance, *J. Geophys. Res.*, *112*, D13211, doi:10.1029/2006JD007811.

Mishchenko, M. I. (2002), Vector radiative transfer equation for arbitrarily shaped and arbitrarily oriented particles: A microphysical derivation from statistical electromagnetics, *Appl. Opt.*, *41*, 7114–7134.

Mishchenko, M. I., and L. D. Travis (1994), *T*-matrix computations of light scattering by large spheroidal particles, *Opt. Commun.*, *109*, 16–21.

Mishchenko, M. I., et al. (1997), Modeling phase functions for dustlike tropospheric aerosols using a shape mixture of randomly oriented polydisperse spheroids, *J. Geophys. Res.*, *102*, 16,831–16,847.

Nakajima, T., and M. D. King (1990), Determination of the optical thickness and effective particle radius of clouds from reflected solar radiation measurements. part I: Theory, *J. Atmos. Sci.*, *47*, 1878–1893.

Omar, A. H., et al. (2005), Development of global aerosol models using cluster analysis of Aerosol Robotic Network (AERONET) measurements, *J. Geophys. Res.*, *110*, D10S14, doi:10.1029/2004JD004874.

O'Neill, N. T., T. F. Eck, A. Smirnov, B. N. Holben, and S. Thulasiraman (2003), Spectral discrimination of coarse and fine mode optical depth, *J. Geophys. Res.*, *108*(D17), 4559, doi:10.1029/2002JD002975.

Remer, L. A., and Y. J. Kaufman (1998), Dynamic aerosol model: Urban/industrial aerosol, *J. Geophys. Res.*, *103*, 13,859–13,871.

Remer, L. A., et al. (2005), The MODIS aerosol algorithm, products, and validation, *J. Atmos. Sci.*, *62*(4), 947–973.

Tanré, D., M. Hermon, and Y. J. Kaufman (1996), Information on aerosol size distribution contained in solar reflectance spectral radiances, *J. Geophys. Res.*, *101*, 19,043–19,060.

Taubman, B. F., J. C. Hains, A. M. Thompson, L. T. Marufu, B. G. Doddridge, J. W. Stehr, C. A. Piety, and R. R. Dickerson (2006), Aircraft vertical profiles of trace gas and aerosol pollution over the mid-Atlantic U. S.: Statistics and meteorological Cluster analysis, *J. Geophys. Res.*, *111*, D10S07, doi:10.1029/2005JD006196.

Volten, H., O. Munoz, E. Rol, J. F. de Haan, W. Vassen, J. W. Hovenier, K. Muinonen, and T. Nousiainen (2001), Scattering matrices of mineral aerosol particles at 441.6 nm and 632.8 nm, *J. Geophys. Res.*, *106*, 17,375–17,401.

Wiscombe, W. J. (1981), Improved Mie scattering algorithms, *Appl. Opt.*, *19*, 1505–1509.

Yang, P., and K. N. Liou (1996), Geometric-optics-integral-equation method for light scattering by nonspherical ice crystals, *Appl. Opt.*, *35*, 6568–6584.

Yu, H., et al. (2006), A review of measurement-based assessments of aerosol direct radiative effect and forcing, *Atmos. Chem. Phys.*, *6*, 613–666.

O. Dubovik, Laboratoire d'Optique Atmospherique, Université des Sciences et Technologies de Lille, F-59655 Villeneuve d'Ascq, France.

R. C. Levy, Science Systems and Applications Inc., NASA Goddard Space Flight Center, Code 613.2, Greenbelt, MD 20771, USA. (levy@climate.gsfc.nasa.gov)

L. A. Remer, Laboratory for Atmospheres, NASA Goddard Space Flight Center, Greenbelt, MD 20771, USA.